9th Asia-Pacific Conference on Wind Engineering
Auckland, New Zealand
3-7 December 2017

# Momentum and Scalar Transport in Inflow Turbulence Generated by Linear Forcing and PID Control

**H. Suto[1], Y. Hattori[1] and K. Nakao[1]**

[1]Civil Engineering Research Laboratory
Central Research Institute of Electric Power Industry, 1646 Abiko, Abiko, Chiba 270-1194, Japan

## Abstract

A method combining extended linear forcing and proportional-integral-differential (PID) control was proposed to provide suitable inflow turbulence conditions in large-eddy simulations of spatially developing boundary layer flows. A PID algorithm controls the mean profiles of the flow and a passive scalar (such as a potential temperature with a small variation), while the forcing superimposes turbulence on the mean flow for fitting turbulence characteristics to previously assumed conditions. The numerical results showed that the characteristics of the flow and scalar transport generated by the method were close to those previously assumed. Moreover, it was suggested that the turbulence characteristics inside a boundary layer vary with the energy-containing scale of the turbulence in the upper air.

## Introduction

The generation of inflow turbulence is of great importance in large-eddy simulations (LESs) of spatially developing flows in nature and industrial applications. Most existing methods of creating a realistic inlet boundary condition for turbulent flows can be broadly divided into two types: (a) the synthesized turbulence methods based on turbulence statistics, such as the inverse Fourier transform (e.g., [1-3]), and (b) the precursor simulation methods based on the conservation equations of fluid dynamics (e.g., [4-7]). The former type has the advantage of the ability to easily specify turbulence parameters, such as turbulent energy levels and length scales, while the latter type has the ability to more correctly reproduce turbulence properties (see [8,9] for more details and properties of these methods). Methods that simultaneously satisfy the two requirements, however, have not been well established.

Focusing on the atmospheric surface layer as a spatially developing flow, on the other hand, the effects of large-scale eddies in the upper air on the coherent motion in the logarithmic layer, which are universally found in wall-bounded turbulent flows even with a high Reynolds number, have been discussed and remain a topic of interest (e.g., [10,11]). The characteristics of the turbulent boundary layer below a turbulent free stream, which appears to be similar to the atmospheric surface layer, have also been investigated from the viewpoint of industrial applications such as blade wakes in turbomachinery (e.g., [12,13]).

This study aims to generate inflow turbulence for LESs of spatially developing atmospheric surface layers. First, a method combining extended linear forcing [14] and proportional-integral-differential (PID) control is proposed. A PID algorithm controls the mean profiles of the flow and a passive scalar (such as a potential temperature with a small variation) in the method, while the forcing superimposes turbulence on the mean flow to enable the fitting of turbulence characteristics to previously assumed conditions. Then, the characteristics of the flow and passive scalar transport generated by this method are investigated to clarify the feasibility of this method as an approach to inflow turbulence generation.

## Numerical Method

The governing equations used in the simulation are the grid-filtered continuous, Navier–Stokes, and passive scalar transport equations,

$$\frac{\partial \langle u_\mathrm{j} \rangle}{\partial x_\mathrm{j}} = 0, \tag{1}$$

$$\frac{\partial \langle u_\mathrm{i} \rangle}{\partial t} + \frac{\partial \langle u_\mathrm{j} \rangle \langle u_\mathrm{i} \rangle}{\partial x_\mathrm{j}} = -\frac{1}{\rho}\frac{\partial \langle p \rangle}{\partial x_\mathrm{i}} + \nu \frac{\partial^2 \langle u_\mathrm{i} \rangle}{\partial {x_\mathrm{j}}^2} - \frac{\partial \tau_\mathrm{ij}}{\partial x_\mathrm{j}} + F_{T\mathrm{ij}} + F_{M\mathrm{i}}, \tag{2}$$

$$\frac{\partial \langle \theta \rangle}{\partial t} + \frac{\partial \langle u_\mathrm{j} \rangle \langle \theta \rangle}{\partial x_\mathrm{j}} = a \frac{\partial^2 \langle \theta \rangle}{\partial {x_\mathrm{j}}^2} - \frac{\partial q_\mathrm{j}}{\partial x_\mathrm{j}} + F_{M\theta}. \tag{3}$$

The source terms of $F_{T\mathrm{ij}}$, $F_{M\mathrm{i}}$, and $F_{M\theta}$ are respectively for turbulence generation by linear forcing, for the PID control of the mean velocity, and for the PID control of the mean scalar:

$$F_{T\mathrm{ij}} = \left( \langle u_\mathrm{j} \rangle - \overline{\langle u_\mathrm{j} \rangle}^\mathrm{T} \right) A_\mathrm{ij}, \tag{4}$$

$$F_{M\mathrm{i}} = K_P \Delta \overline{\langle u_\mathrm{i} \rangle}^\mathrm{L} + K_I \int_0^t \Delta \overline{\langle u_\mathrm{i} \rangle}^\mathrm{L} d\tau + K_D \frac{\partial \Delta \overline{\langle u_\mathrm{i} \rangle}^\mathrm{L}}{\partial t}, \tag{5}$$

$$F_{M\theta} = K_{P\theta} \Delta \overline{\langle \theta \rangle}^\mathrm{L} + K_{I\theta} \int_0^t \Delta \overline{\langle \theta \rangle}^\mathrm{L} d\tau + K_{D\theta} \frac{\partial \Delta \overline{\langle \theta \rangle}^\mathrm{L}}{\partial t}. \tag{6}$$

$u_i$: velocity in $i$ direction, $t$: time, $\rho$: density, $p$: pressure, $\nu$: kinematic viscosity, a: thermal diffusivity, $\tau_{ij}$: subgrid-scale (SGS) stress tensor, $q_i$: SGS scalar flux, $A_\mathrm{ij}$: linear forcing coefficient (tensor), $K_P, K_I, K_D, K_{P\theta}, K_{I\theta}, K_{D\theta}$: PID control coefficients $(= 1\times10^3, 1\times10^3, 0, 1\times10^3, 1\times10^3, 0)$, $\langle\ \rangle$: value at grid scale (GS), $\bar{f}^\mathrm{T}$: time-averaged value of $f$ within time scale $T$, $\bar{f}^\mathrm{L}$: spatially averaged value of $f$ within horizontal area of $L^2 (= Lx \cdot Lz)$ at arbitrary height, $Lx, Lz$: domain size in $x$, $z$ directions, $\Delta f$: deviation from target value $f_0$ $(= f - f_0)$. The length scale of turbulence generated by using the original linear forcing proposed by Lundgren [15] depends on the domain size [16], while Equation (4) allows one to expand the range of the length scale of the turbulence to be generated by using a time-averaged velocity within a time scale [14] instead of a constant velocity, which is assumed in the original linear forcing. $\tau_{ij}$ and $q_i$ are treated by the Smagorinsky model (the Smagorinsky constant and the SGS turbulent Schmidt number are set at 0.1 and 0.5, respectively). The governing equations are discretized by the second-order central differencing method and the second-order Adams-Moulton method.

On the assumption of the balance between the production and dissipation of the turbulence kinetic energy and sufficiently small SGS Reynolds stresses, the linear forcing coefficient $A_\mathrm{ij}$ is related to the flow properties as

$$\overline{\langle u_\mathrm{i} \rangle' \langle u_\mathrm{j} \rangle'}^\mathrm{L} A_\mathrm{ij} = \varepsilon - \overline{\langle u_\mathrm{i} \rangle' \langle u_\mathrm{j} \rangle'}^\mathrm{L} \frac{\partial \overline{\langle u_\mathrm{i} \rangle}^\mathrm{L}}{\partial x_\mathrm{j}}. \tag{7}$$

$\varepsilon$: dissipation rate. Moreover, assuming the generation of isotropic turbulence, i.e., the diagonal elements of $A_\mathrm{ij}$ have the same value

$A_{\mathrm{iso}}$ and the off-diagonal elements are zero, the following equation is obtained:

$$A_{\mathrm{iso}} \equiv A_{\mathrm{ii}} = \frac{1}{\langle \mathrm{u_i}\rangle'\langle \mathrm{u_i}\rangle'^{\mathrm{L}}}\left(\varepsilon - \overline{\langle u_{\mathrm{k}}\rangle'\langle u_{\mathrm{l}}\rangle'}^{\mathrm{L}}\frac{\partial\overline{\langle u_{\mathrm{k}}\rangle}^{\mathrm{L}}}{\partial \mathrm{x_l}}\right). \quad (8)$$

On the other hand, assuming the generation of anisotropic turbulence (a simple shear turbulent flow neglecting the advection effects of fluctuating velocities), i.e., only the element $\mathrm{A_{12}}$ has a value $\mathrm{A_{aniso}}$ and the other elements are zero, the following equation is obtained:

$$A_{\mathrm{aniso}} \equiv \mathrm{A_{12}} = \frac{1}{\langle \mathrm{u_1}\rangle'\langle \mathrm{u_2}\rangle'^{\mathrm{L}}}\left(\varepsilon - \overline{\langle u_{\mathrm{k}}\rangle'\langle u_{\mathrm{l}}\rangle'}^{\mathrm{L}}\frac{\partial\overline{\langle u_{\mathrm{k}}\rangle}^{\mathrm{L}}}{\partial \mathrm{x_l}}\right). \quad (9)$$

Figure 1 shows the computational domain used. A turbulent shear layer on a flat wall with mean flow in the *x* direction is assumed. In the source terms $F_{M\mathrm{i}}$, $F_{M\theta}$ (Equations (5) and (6)), the following empirical equation [17] and linear function are given for the target velocity and target passive scalar (assuming a potential temperature with a small variation), respectively:

$$\frac{u_0}{u_\infty} = \min\left(\frac{u_\tau}{u_\infty}\left[\frac{1}{\kappa}ln\left(\frac{y}{\frac{\nu}{u_\tau}}\right) + B + \frac{2\Pi}{\kappa}sin^2\left(\frac{\pi}{2}\frac{y}{\delta}\right) - F\right], 1\right)$$

$$\text{for } \frac{y}{\frac{\nu}{u_\tau}} \geq 30, \quad (10)$$

$$\frac{\theta_0}{\theta_\infty} = \min\left(\frac{y}{\delta}, 1\right). \quad (11)$$

$u_\infty, \theta_\infty$: mean velocity and mean scalar in upper flow, $u_\tau$: friction velocity, $\kappa$: von Karman constant (=0.41), $B = 5.0$, $\Pi = 0.55$, $F = 0.0$. The function min( ) gives the minimum value. $F_{M\mathrm{i}}$ is set to zero when $y/(\nu/u_\tau) < 30$. Moreover, as an attempt to mimic overlying large-scale eddies (detached eddies) on real atmospheric surface layers [11], the source term $F_{T\mathrm{ij}}$ (Equation (4)) is given only in the upper region of $0.6\delta \leq y \leq Ly$, in which the velocity gradient is zero (Equation (10)). Namely, the terms including $\partial\overline{\langle u_{\mathrm{k}}\rangle}^{\mathrm{L}}/\partial \mathrm{x_l}$ in Equations (8) and (9) are zero. The free-slip and zero-scalar-flux conditions, no-slip and constant-scalar conditions, and periodic condition are applied at the upper boundary (y = Ly), lower boundary (y = 0), and side boundaries ( x = 0, Lx ; z = 0, Lz ), respectively. The calculations are performed using the values nondimensionalized with $u_\infty$, $\theta_\infty$, and $\delta$ and the coordinate system moving with the velocity $u_\infty$.

Table 1 shows the computational conditions. The time-averaging length of "∞" corresponds to the case that $\overline{\langle u_{\mathrm{l}}\rangle}^{\mathrm{T}}$ in Equation (4) is constant. The energy dissipation rate $\varepsilon$, i.e., the energy input to the system, is set at a constant value. $\overline{\langle \mathrm{u_i}\rangle'\langle \mathrm{u_i}\rangle'}^{\mathrm{L}}$ and $\overline{\langle \mathrm{u_1}\rangle'\langle \mathrm{u_2}\rangle'}^{\mathrm{L}}$ in Equations (8) and (9) are calculated by using the velocities at each time step [14]. The open-source code FrontFlow/red (Ver.3.1) is used for this numerical simulation.

## Results and Discussion

### *Instantaneous Field*

First, we outline the flow and scalar fields generated by this method. Figure 2 shows the distributions of the instantaneous velocity vector $(u/u_\infty - 1, v/u_\infty)$ and the instantaneous scalar contour in an *x*-*y* plane (those in cases 3 and 4 are omitted). The magnitude of the velocity is represented by the color of the vectors (the length of the vectors does not have a physical meaning). The vertical velocity gradient, which should be generated by the PID control in both cases, can be found in the region $y/\delta \leq 1$. On the other hand, the flow in the region $1 \leq y/\delta$ changes with the forcing: the velocity is almost zero in case 1 without the forcing, while the fluctuation appears clearly in case 2 with the forcing.

### *Vertical Structure*

Next, the vertical structures of the generated flow and scalar are quantitatively observed. Figure 3 shows the vertical distributions of the mean velocity and mean scalar in cases 1 and 2 (those in cases 3 and 4 are omitted, which have similar results). The vertical axis is normalized by $\delta$, and the horizontal axis is normalized by $u_\tau$ and $\theta_\infty$. The values in both cases are in good agreement with the target distribution (target), indicating that the PID control functions effectively.

| Case | Domain size *Lx/δ*, *Ly/δ*, *Lz/δ* | Number of grid points *nx*, *ny*, *nz* | Grid resolution *dx/δ*, $dy_{\min}/\delta$, $dy_{\max}/\delta$, *dz/δ* | Forcing coefficient $A_{\mathrm{ij}}$ | Energy dissipation $\varepsilon$ | Time-averaging length *T* | Kinetic viscosity *ν* |
|---|---|---|---|---|---|---|---|
| 1 | 4, 5, 4 | 58, 81, 51 | 0.05, 0.01, 0.1, 0.05 | 0 | - | - | $1.0\times10^{-4}$ |
| 2 | 4, 5, 4 | 58, 81, 51 | 0.05, 0.01, 0.1, 0.05 | $A_{\mathrm{iso}}$ | $5.0\times10^{-4}$ | ∞ | $1.0\times10^{-4}$ |
| 3 | 4, 5, 4 | 58, 81, 51 | 0.05, 0.01, 0.1, 0.05 | $A_{\mathrm{iso}}$ | $5.0\times10^{-4}$ | 2 | $1.0\times10^{-4}$ |
| 4 | 4, 5, 4 | 58, 81, 51 | 0.05, 0.01, 0.1, 0.05 | $A_{\mathrm{aniso}}$ | $5.0\times10^{-4}$ | ∞ | $1.0\times10^{-4}$ |

Table 1. Computational conditions.

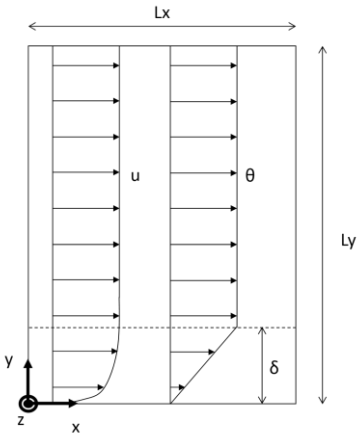


Figure 1. Computational domain.

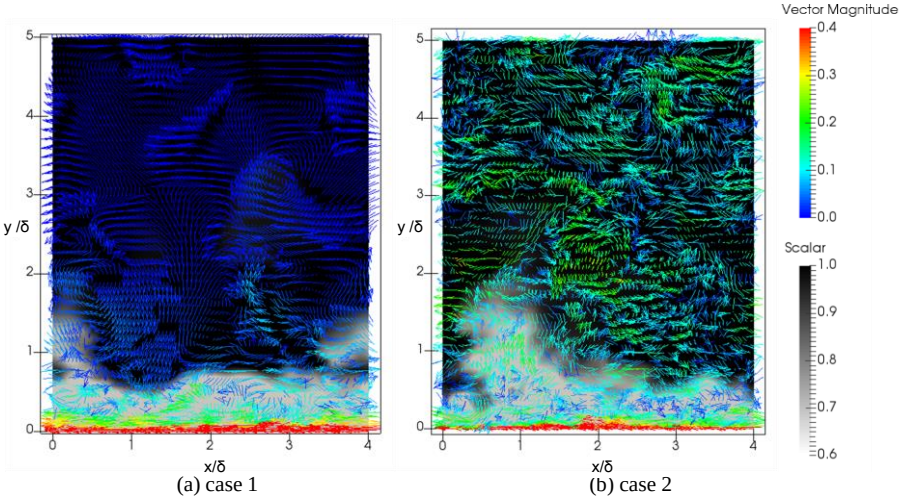


(a) case 1 (b) case 2

Figure 2 Instantaneous velocity vectors of $(u/u_\infty - 1, v/u_\infty)$ in a *x*-*y* plane.

Figures 4 and 5 respectively show the vertical distributions of the rms velocity and rms scalar. Regarding the rms velocity, there are clear variations between the cases in the upper flow ($1 \leq y/\delta$): the rms velocity increases with forcing (cases 1 and 2), the rms velocity decreases with decreasing averaging time $T$ (cases 2 and 3), and the $u$ component of the rms velocity relatively increases with anisotropic forcing (cases 2 and 4). Moreover, as mentioned in Hancock and Bradshaw [12], the turbulence in the upper flow affects the inside of the boundary layer ($y/\delta \leq 1$), causing the rms velocity to increase (in cases 2 and 4) or decrease (in case 3). The rms scalar inside the boundary layer is also influenced by the disturbance in the upper flow and shows a similar increase or decrease to the rms velocity. However, the rms scalar is small in the upper flow since the gradient of the mean scalar, i.e., the generation of the rms scalar is zero there.

Figure 6 shows the vertical distribution of the Reynolds stress (the turbulent scalar flux is omitted, which has a similar trend to the rms scalar). It is found that the difference in the Reynolds stress between cases 1-3 is small. Note that the experiment of Hancock and Bradshaw [12] shows that the Reynolds stress inside the boundary layer decreases owing to the turbulence in the upper flow and does not correspond to the trend observed in this figure. The variation in the profile of the mean velocity in the experiment, such as the decrease in the wake region in the boundary layer, might have caused this inconsistency. It is also noted that the Reynolds stress in the upper flow has a significant value only in case 4 with anisotropic forcing.

### *Turbulence Scale*

Finally, to observe the variation in the turbulence scale between the cases, the ratio of the turbulence scale $l$ $(= (2/3k)^{3/2}/\varepsilon$, $k = ({u_{rms}}^2 + {v_{rms}}^2 + {w_{rms}}^2)/2$ ), which corresponds to the energy-containing turbulence scale, to the layer height $\delta$ is shown in Figure 7. In the upper flow, the scale $l$ in cases 2-4 with forcing has significant values. Here, note that the scale $l$ in the upper flow in cases 2 and 4 with the longer averaging time is larger than that inside the boundary layer. At this time, the scale $l$ inside the boundary layer, in which forcing is not performed, is increased compared with that in case 1, as well as the rms velocity and rms scalar (Conversely, in case 3, the scale $l$ inside the boundary layer is decreased owing to the small-scale disturbance added in the upper flow). This suggests that the characteristics of turbulence

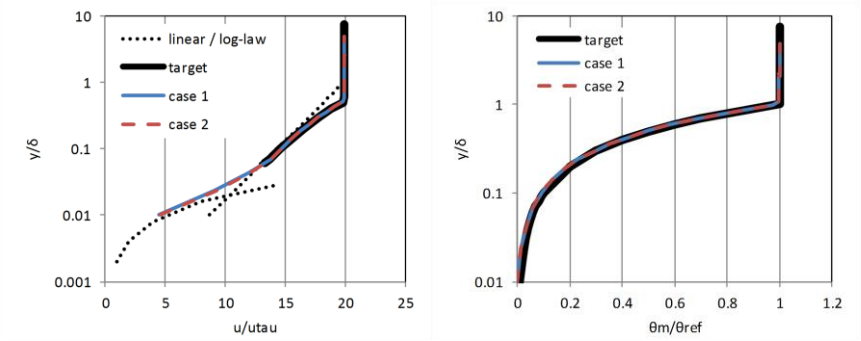


(a) mean velocity (b) mean scalar

Figure 3. Vertical distribution of mean velocity and mean scalar (comparison between cases 1 and 2).

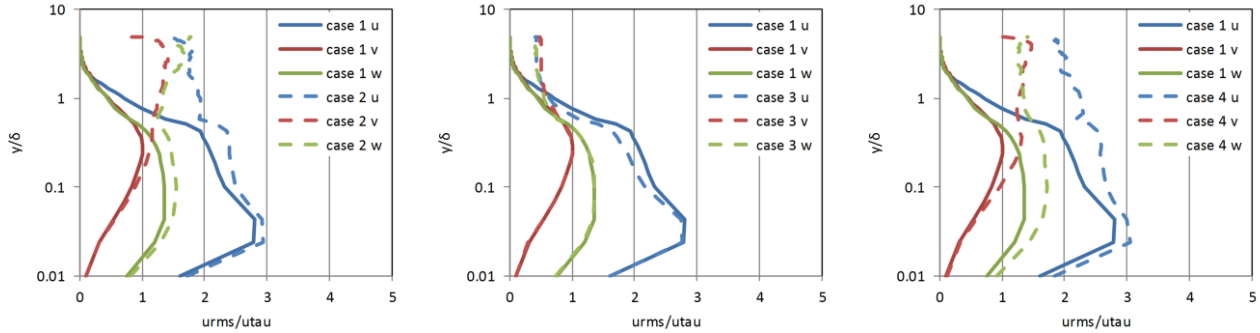


(a) case 2 (b) case 3 (c) case 4

Figure 4. Vertical distribution of rms velocity (comparison with case 1)

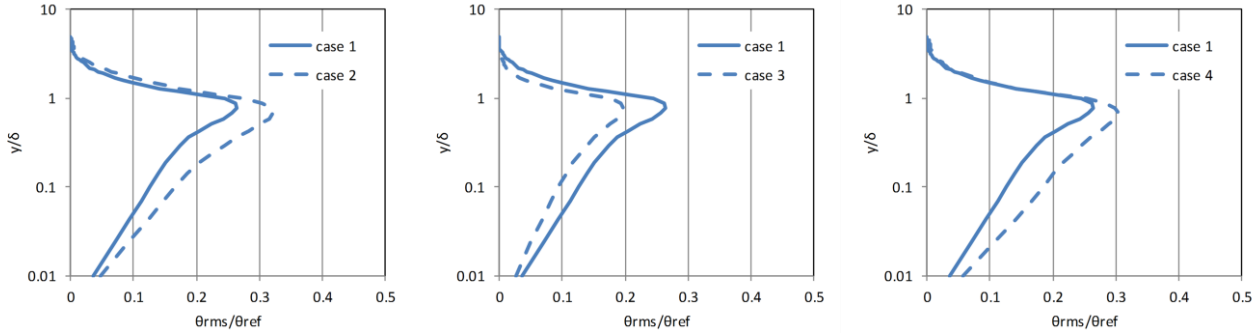


(a) case 2 (b) case 3 (c) case 4

Figure 5. Vertical distribution of rms scalar (comparison with case 1)

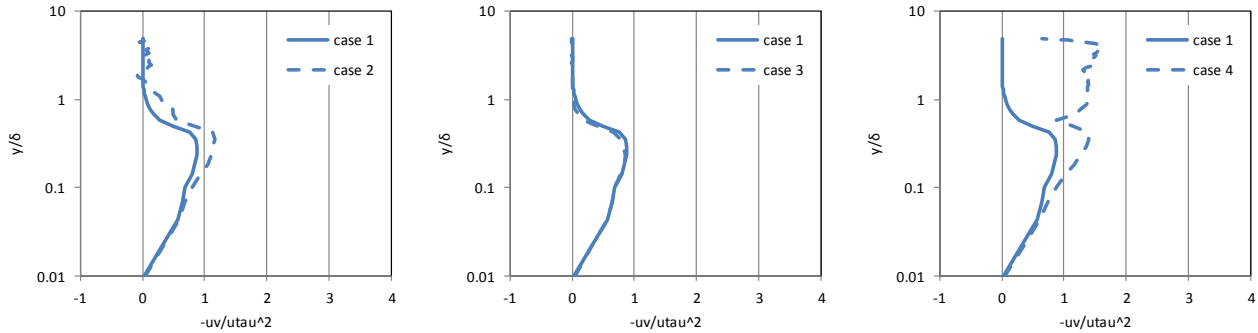


(a) case 2 (b) case 3 (c) case 4

Figure 6. Vertical distribution of Reynolds stress (comparison with case 1).

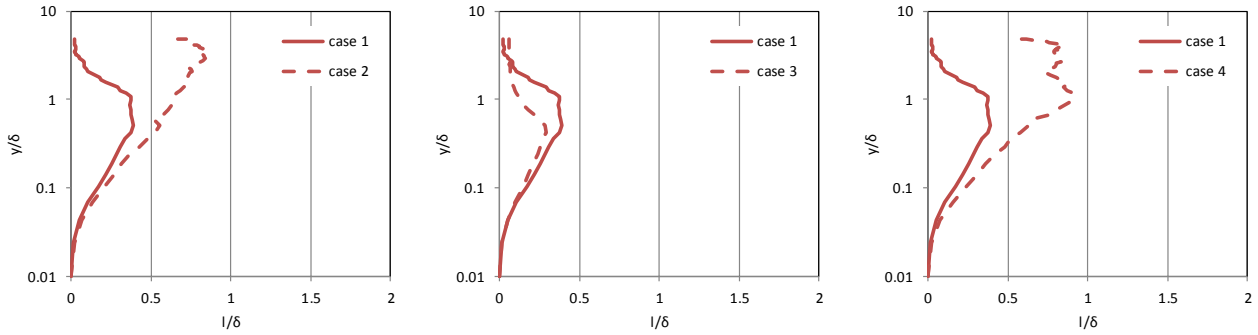


(a) case 2 (b) case 3 (c) case 4

Figure 7. Vertical distribution of turbulence scale $l$ (comparison with case 1).

inside a turbulent boundary layer vary with the energy-containing turbulence scale in the upper flow.

## Conclusions

Four typical numerical results obtained with different forcing parameters showed that the characteristics of the flow and passive scalar transport generated by the proposed method are close to those previously assumed. Moreover, it was suggested that the turbulence characteristics inside a boundary layer vary with the energy-containing turbulence scale in the upper flow. Although it was also confirmed that the results in this paper are similar to the features of the atmospheric surface layer, which have been revealed by experiments and observations, a detailed comparison and clarification of the phenomena will be reported in the future.

## Acknowledgments

This study utilized the results of the research and development project of revolutionary simulation software of MEXT and the results of research at Hokkaido University.

## References

[1] Kondo, K., Murakami, S. & Mochida, A., Generation of velocity fluctuations for inflow boundary condition of LES, *J. Wind Eng. Ind. Aerodyn.*, **67-68**, 1997, 51–64.

[2] Maruyama, T., Rodi, W., Maruyama, Y. & Hiraoka, H., Large eddy simulation of the turbulent boundary layer behind roughness elements using an artificially generated inflow, *J. Wind Eng. Ind. Aerodyn.*, **83**, 1999, 381–392.

[3] Huang, S. H., Li, Q. S. & Wu, J. R., A general inflow turbulence generator for large eddy simulation, *J. Wind Eng. Ind. Aerodyn.*, **98**, 2010, 600–617.

[4] Lund, T. S., Wu, X. & Squires, K. D., Generation of turbulent inflow data for spatially-developing boundary layer simulations, *J. Comput. Phys.*, **140**, 1998, 233–258.

[5] Nozawa, K. & Tamura, T., Large eddy simulation of the flow around a low-rise building immersed in a rough-wall turbulent boundary layer, *J. Wind Eng. Ind. Aerodyn.*, **90**, 2002, 1151–1162.

[6] Liu, K. L. & Pletcher, R. H., Inflow conditions for the large eddy simulation of turbulent boundary layers: a dynamic recycling procedure, *J. Computat. Phys.*, **219**, 2006, 1–6.

[7] Araya, G., Castillo, L., Meneveau, C. & Jansen, K., A dynamic multi-scale approach for turbulent inflow boundary conditions in spatially developing flows, *J. Fluid Mech.*, **670**, 2011, 581–605.

[8] Keating, A., Piomelli, U., Balaras, E. & Kaltenbach, H.-J., A priori and a posteriori tests of inflow conditions for large-eddy simulation, *Phys. Fluids*, **16**, 2004, 4696–4712.

[9] Tabor, G. R. & Baha-Ahmadi, M. H., Inlet conditions for large eddy simulation: a review, *Comput. Fluids*, **39**, 2010, 553–567.

[10] Högström, U., Hunt, J. C. R. & Smedman, A S., Theory and measurements for turbulence spectra and variances in the atmospheric neutral surface layer, *Boundary Layer Meteorol.*, **103**, 2002, 101–124.

[11] Hattori, Y., Moeng, C.-H., Suto, H., Tanaka, N. & Hirakuchi, H., *Boundary Layer Meteorol.*, **134**, 2010, 269–283.

[12] Hancock, P. E. & Bradshaw, P., Turbulence structure of a boundary layer beneath a turbulent free stream, *J. Fluid Mech.*, **205**, 1989, 45–76.

[13] Blair, M. F., Influence of free-stream turbulence on turbulent boundary layer heat transfer and mean profile development, Part II-Analysis of results, *J. Heat Transfer*, **105**, 1983, 41-47.

[14] Suto, H., Hattori, Y. & Nakao, K., A specification method of turbulence length scale for inflow turbulence generation using linear forcing, *Proc. 23rd National Symp. Wind Engineering*, Tokyo, 2014, 469–474 (in Japanese).

[15] Lundgren, T. S., Linearly forced isotropic turbulence, in *Annual Research Briefs*, Center for Turbulence Research, Stanford, 2003, 461–473.

[16] Rosales, C. & Meneveau, C., Linear forcing in numerical simulations of isotropic turbulence: Physical space implementations and convergence properties, *Phys. Fluids*, **17**, 2005, 095106.

[17] Coles, D., The law of the wake in the turbulent boundary layer, *J. Fluid Mech.*, **1**, 1956, 191–226.